A CYBER-PHYSICAL OBSERVER FOR FLUIDIZED BED CHEMICAL LOOPING PROCESS DEVELOPMENT

Lawrence J. Shadle[1*], Samuel Bayham[1], David Tucker[1], Paolo Pezzini[1,2], Esmail Monazam[1,3], Justin Weber[1], Ronald Breault[1], Mark Bryden[2]

[1]*National Energy Technology Laboratory, 3610 Collins Ferry Rd, Morgantown, WV, USA 26507-0880*

[2]*Simulation Modeling and Decision Science Program, Ames Laboratory, U.S. Department of Energy, Iowa State University, 1620 Howe Hall, Ames, IA 50011*

[3] *REM Engineering Services, Collins Ferry Rd, Morgantown, WV, USA 26507-0880*

*Email: *lshadl@netl,doe.gov*

Abstract –A cyber-physical observer (CPO) is under development to control the operations of a fluidized bed-chemical looping reactor (FB-CLR) pilot plant. The cyber-physical approach is a novel means to combine computational modeling with hardware to integrate complex components in a dynamic fashion. Experience from pilot plant operations is that control of the solids flows and bed inventories are often challenging and may result in the need to reload oxygen carrier particles multiple times during a weeklong test campaign. The solids transfer between process units in coupled fluidized bed systems cannot be simulated with sufficient speed or accuracy to identify slugging, choking, flooding, or the hysteresis events that can occur near incipient fluidization leading to flow disruption/reversal that upset process operations. The CPO is being designed to duplicate, or mirror, the multiphase flow system in real time hardware.

INTRODUCTION

Because of the greater demands on the emissions and efficiency, advanced power systems are beginning to resemble highly coupled chemical process plants. Computational modeling has provided the ability to evaluate various process configurations, dynamic effects of coupling process systems, and even the local dynamics of changes in process geometries. While these changes have made significant contributions to our understanding of the processes that we develop they have not yet reached their full potential, nor have they significantly sped up development time. One only needs to look at the development time table and cost overruns for new processes at the Pinon Pine and Kemplar power plants, or radioactive waste storage at Hanford to conclude that we could benefit from a new approach to our research and development. In research areas where progress is rapid and development time is critical to viability, such as information technology, automotive industry and healthcare, a cyber-physical approach has gained favor.

Cyber-physical systems include process models which interact in real time with hardware, obtaining input from sensors and sending commands to control valve actuators in response. Cyber-physical systems can be applied to energy research to speed development of highly efficient power systems by: 1) evaluating immature technologies, 2) working out technology integration issues, 3) identifying potential applications and research needs, 4) optimizing system performance, and 5) developing and demonstrating process controls. A cyber-physical system is comprised of computational models and controllers making up the cyber part, and physical hardware and actuators that are the physical parts. These diverse components are integrally coupled through flows, sensors, and control hardware. This is demonstrated by examining the detail of a cyber-physical experiment.

Tucker et al. (2005 and 2014) built the first cyber-physical model of an advanced power system in order to evaluate the potential for turbine-fuel cell hybrid power prior to the availability of fuel cells for this type of service. The principal hardware in the Hyper is a gas turbine and compressor sharing a single shaft. This turbine experimentally responds to changes in a dynamic model of a solid oxide fuel cell. Thus in addition to the connection in software of the power produced by the fuel cell, the individual components are also coupled thermally and aerodynamically. The air flow from the compressor is preheated by passing through a heat exchanger, recuperator, before flowing into the pressure vessel designed to house the solid oxide fuel cell fuel (physical parts). The chemistry in the fuel cell is simulated (cyber part) and its resulting heat output is used to control the fuel valve on a natural gas fired combustor directly downstream of the fuel cell's pressure vessel. The mass and heat flow from this cyber-physical fuel cell model is directed into, and is expanded across, the gas turbine thereby producing power. Before exhausting the gas to the atmosphere, the residual heat is

extracted when it passes through the recuperator (additional physical parts), thereby completing the hybrid loop.

There is great potential to use other cyber-physical systems for energy technology development. A cyber-physical observer is proposed to aid development of chemical looping reactor (CLR) technology (Shadle et al., 2017). The CLR is reported (Richards et al., 2014) to achieve carbon management and simplify CO_2 sequestration by eliminating the need for oxygen enrichment. NETL has built an integrated fluid bed chemical looping reactor (FB-CLR). Fluidized beds are employed in the CLR because of their potential to transfer the solids with low parasitic power requirements, as well as their distinct technological advantages of good gas-solid contact, mixing, and heat transfer. However, the NETL FB-CLR exhibited complex gas and solids flow behavior that has been difficult to control. One of the key observations has been the inability to maintain a constant inventory and solids flow rates in the CLR. This may be due to any one of a number of potential causes. Several changes to process cyclones and the downstream pressure, temperature and particulate control systems have improved operability, but performance has remained marginal.

An integral part of the gas solids separation system in NETL'S FB-CLR is a fluidized bed Seal Pot that is used to minimize leaking vitiated air from the Air Reactor into the CO_2 stream produced in the Fuel Reactor. One of the critical remaining issues is establishing and controlling the desired flow paths where multiple outlet paths exist. Exhaust flow direction is determined by several interdependent factors including the back pressure control valve position and control strategy, the relative drag or loading on the barrier filters, and the relative heights of different columns of granular materials separating the gas exits. The goal is to improve the seals between reactors, system routine operations, and avoid process upsets spoiling the cyclone separators. Unfortunately, solids transfer between fluidized bed systems cannot be simulated with sufficient speed or accuracy to identify slugging, choking, flooding, or the hysteresis events that can occur near incipient fluidization leading to flow disruption/reversal that upset process operations. A cyber-physical FB-CLR is being developed to investigate the causes of these problems and observe and control the multiphase flow behavior. The first step in creating this observer is to evaluate the process states. In this paper, scaling is investigated and a mass and pressure balance is analyzed with the intention of identifying the process states along with the control parameters and their sensitivity towards maintaining operational stability.

At NETL we have the opportunity to use an existing cold unit as an observer to aid in the operations and control of an operational hot test unit of the same dimensions. The cyber-physical observer will receive information from the hot unit on the pressure, temperatures, and flows. This stimulus will provide input to reaction models and scaling relationships to provide set-points to the cold flow unit actuators. Taken in conjunction with the measured responses from the cold flow unit sensors, such as the bed heights and solids flows, the observer will provide set points for the pilot scale hot unit CLR to ensure stable operations and smooth transitions.

An observer for process control is used to estimate unmeasurable states while it is running in real-time. Luemberger and Kalman filters are the most commonly used methods to estimate these states from measurable system inputs and outputs. Luemberger uses a deterministic approach whereas the Kalman employs a stochastic method of minimizing the differences between the estimated and measurable outputs from the system. Shadle et al. (2017) describe the algebraic model for the input/output in this observer and discuss the control architecture between the hot and the cold unit.

EXPERIMENTAL METHODS

A schematic of the FB-CLR system is shown in Fig 1. The oxygen carrying solid particles were fluidized in the Fuel Reactor with a preheated stream of nitrogen. This simplified the experimental operations; in a commercial operation, the nitrogen would be replaced with a recycle stream of CO_2 and steam. This fluidizing gas was introduced through a gas distributor across the bottom of the fluid bed to mix the reactants. Methane was injected into the Fuel Reactor bed above the gas distributor, and when temperatures reach 800 C, produced CO_2 and water according to the following chemical reaction:

$$CH_4 + 4M_xO_y \underset{\Delta}{\rightarrow} CO_2 + 2H_2O + 4M_xO_{y-1} \quad (1)$$

where M is a metal combined with oxygen such as Fe_2O_3, CuO, or NiO, and x and y denote the stoichiometry and oxidation state of the carrier. The gaseous products of combustion were exhausted from the Fuel Reactor through a side port and particulate was separated by a barrier filter prior to pressure letdown through a back-pressure control valve. The reduced carrier was conveyed to the oxidizer, i.e. Air Reactor, through a non-mechanical valve, L-valve, by means of an underflow port. Solids flow through the L-valve was controlled using two side wall ports in the vertical leg and a sparger. The L-valve aeration in the vertical leg assisted solids movement into the horizontal leg, while the sparger fluidized the solids there moving them into the Air Reactor. The reduced metal, M, was oxidized in the Air Reactor according to Eq. 2.

$$4M_xO_{y-1} + 2(O_2 + 3.73N_2) \xrightarrow{\Delta} 4M_xO_y + 7.52\,N_2 \quad (2)$$

The Air Reactor was fluidized with preheated air entering through a distributor. The solids entered through a side port near the bottom of this cylindrical unit. Secondary air injection above the solids and on the opposite sidewall transported the oxidized solids up through the riser. The dilute gas solids mixture was further accelerated across the reduced diameter horizontal section and led into a cyclone in which the gas and solids were separated. The vitiated air from the Air Reactor exit the cyclone and passed through a barrier filter before the pressure letdown valve. The oxidized solids fall down the cyclone dipleg to enter the Seal-Pot.

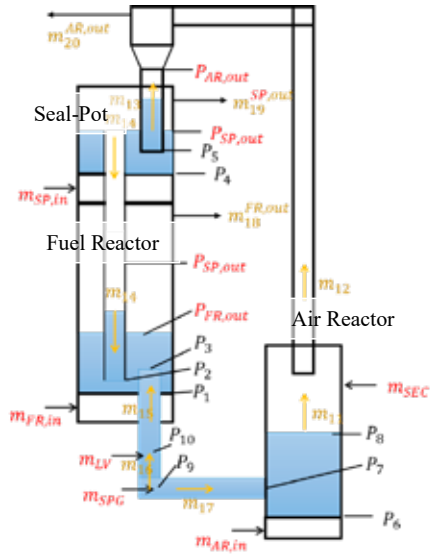

Figure 1 Schematic of FB-CLR with symbols used in mass and pressure balance.

The CLR employs a fluidized bed Seal-Pot to minimize leaking vitiated air from the Air Reactor into the sequestration ready CO_2 stream produced in the Fuel Reactor. The Seal Pot was fluidized with nitrogen through a distributor across its bottom. The fluidizing gas was vented from a side port in the freeboard and then through a barrier filter and back pressure control valve. The cyclone dipleg feeds oxidized solids from the Air Reactor into the Seal Pot, and an overflow pipe transfers those solids to the Fuel Reactor. The moving beds associated with these solids inlets and outlets are displayed in Fig. 2. Thus, the Seal Pot is meant to serve as a self-regulating non-mechanical valve relying on a column of solids to stop gases from flowing in the wrong direction. The fluidizing gas in the Seal-Pot was designed to exhaust through its side port and then passed through a barrier filter and back-pressure control valve. The oxygen carrier particles exited the Seal-Pot through an overflow pipe into the fluidized bed in the Fuel Reactor.

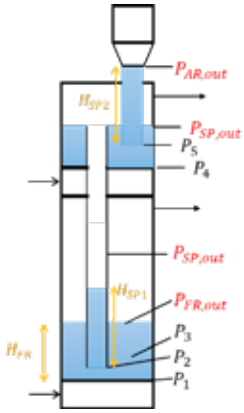

Figure 2. Standpipe moving bed heights associated with Seal-Pot.

Nominally, 50 kg of oxygen carrier was loaded into the hot FB-CLR. The CLR is an atmospheric test vessel; however, the pressures in the Fuel Reactor, Loopseal, and at the exit of the primary cyclone are controlled in order to establish flows and flow path while avoiding flow reversals and process upsets. The oxygen carrier properties were measured using standard methods described by Tucker et al. (2012).

MODELING APPROACH

Scaling. In the hot reacting system the incoming flows, temperatures, and oxygen carrier solids inventory are controlled to meet desired test conditions through system start-up, steady state, and shutdown states. The cold flow unit was built to assist in process operations, troubleshooting, and to evaluate process modifications. Several changes in the primary cyclone were evaluated using this cold flow unit. However, in order to do emulate the hydrodynamics found in the hot unit, the flows and responses must be scaled for the cold flow conditions. The approach was to use non-dimensional analysis Ruzicka (2008). The forces relevant depend upon the operating regime. A recent numerical validation of scaling as applied to fluidized beds is provided by Ommen et al. (2016). They describe how Glicksman (1984) successfully identified the following dimensionless parameters for use with gas-solid fluidized beds.

$$\frac{u_g^2}{gL}, \frac{\rho_s}{\rho_g}, \frac{\beta L}{\rho_s u_g}, L, \frac{G_s}{\rho_s u_g}, \frac{P_o}{\rho_s u_g^2} \tag{3}$$

The fluid to particle drag coefficient, β, depends upon the gas velocity and solids concentration. At low velocities and high solids densities it comes from the Ergun Eq. while at high velocities and low solids loadings it is related to single particle drag. In the full set of scaling laws this drag term is replaced by the Reynolds number, $\frac{\rho_g u_g d_p}{\mu}$, and another dimensionless length, $\frac{d_p}{L}$, as long as the sphericity and particle size distributions in the hot and cold units are kept equal. However, the viscous limit set reported by Glicksman (1988) may be the most relevant set of scaling parameters considering that the critical parameter of interest in the cold flow unit are the influence that the heights of the two dense beds on either side of the Seal-Pot may have on the pressure balance.

$$\frac{u_g^2}{gL}, \frac{u_g}{u_{mf}}, \frac{\rho_s}{\rho_g}, \frac{G_s}{\rho_s u_g}, L, \varphi, \ particle\ size\ distribution \tag{4}$$

This set is derived for low flow cases, *Re*<4, where the first term of the Ergun Eq. is dominant in determining the gas-solids drag. This set differs from that reported by Glicksman in a single term, the dimensionless flux has been included, because the solids around this Seal-Pot are being circulated. This results in a fewer number of parameters that must be matched.

Mass and Force Balance. The steady-state pressure balance model consists of the following inputs: Solids inventory, Gas flows, Primary and secondary air, Gas to the fuel reactor (no reaction yet), Nitrogen to seal pot, Nitrogen to aeration and sparger gases, Temperatures of each reactor (to convert mass of gas to volume), Outlet pressure for fuel reactor, air reactor, and seal pot gas outlets. The model consists of a gas mass balance for each reactor (air, fuel, and seal pot) combined with relations for pressure based on solids inventory in each reactor and standpipe. The gas mass balance for each reactor is

$$\frac{dm_g}{dt} = 0 = \dot{m}_{in,plenum} - \dot{m}_{outlet} + \dot{m}_{standpipe,1} + \dot{m}_{standpipe,2} \tag{5}$$

Where $\dot{m}_{in,plenum}$ is the gas into the reactor from the plenum of the fluidized bed, $\dot{m}_{outlet}$ is the gas exiting the reactor through the reactor gas outlet and backpressure control valve, and $\dot{m}_{standpipe,i}$ is the flow entering or exiting the reactor through a standpipe. Even though the flow in the standpipe might be fluidized, the mass flow for each standpipe is calculated based on the frictional pressure drop through a packed bed.

$$\dot{m}_{standpipe} = \rho_g \frac{\Delta P}{R_{SP}} - \frac{\dot{m}_s}{\rho_s(1-\varepsilon)} \tag{6}$$

Where the resistance term R_{SP} comes from the viscous term in Ergun's equation:

$$R_{SP} = \frac{150 H_{SP}(1-\varepsilon)^2 \mu}{\varepsilon^3 d_p^2 A_{SP}} \tag{7}$$

H_{SP} is the height of the standpipe (determined below), ϵ is the packed bed void fraction, μ is the gas viscosity, d_p is the particle size, and A_{SP} is the cross-sectional area of the standpipe. For the horizontal section of the L-valve, the resistance is estimated based on a constant that can be fit from pressure data from the CLR. The pressure drop ΔP comes from a combination of the known static pressures given by the user and the weight and height of solids in a fluidized bed. From these relations, the system of governing equations can be written. The system of equations to determine the pressure balance for the entire system are shown in Table 1, and the sheet of flows is shown in Figure 1.

Table 1. System of governing equations for the system pressure balance. Pressures in bold are known.

$P_1 = \boldsymbol{P_{FR,out}} + \rho_s(1-\varepsilon)gL_{FR,bed}$
$\boldsymbol{P_{SP,out}} - P_2 = \frac{m_{14}}{\rho_g} R_{14}$
$P_2 = P_1 - \rho_s(1-\varepsilon)gL_{FR-2}$
$P_4 = \boldsymbol{P_{SP,out}} + \rho_s(1-\varepsilon)gL_{ZS,bed}$
$P_5 - \boldsymbol{P_{AR,out}} = \frac{m_{13}}{\rho_g} R_{13}$
$P_4 - P_5 = \rho_s(1-\varepsilon)gL_{5-4}$
$P_{10} - P_3 = \frac{m_{15}}{\rho_g} R_{15}$
$P_3 = \boldsymbol{P_{FR,out}} + \rho_g(1-\varepsilon)gL_{FR,out-3}$
$P_9 - P_{10} = \frac{m_{16}}{\rho_g} R_{16}$
$P_9 - P_7 = \frac{m_{17}}{\rho_g} R_{17}$
$P_6 - P_8 = \rho_s(1-\varepsilon)gL_{6-8}$
$P_7 - P_6 = \rho_s(1-\varepsilon)gL_{7-6}$
$P_7 = P_8 - \rho_s(1-\varepsilon)gL_{7-8}$

The pressure balance is also dependent on the heights of solids in the system. The solids inventories in the air reactor and seal pot are relatively constant, and because the diameters of the standpipes in the system are small, it is assumed that the fuel reactor height is the difference between the total solids inventory and the sum of the air reactor and seal pot inventories, namely:

$$H_{FR} = \frac{1}{\rho_B A_{FR}}(m_{inv} - m_{AR} - m_{\mathrm{L-valve}} - m_{SP}) \tag{8}$$

From this mass, the pressure at the bottom of the fuel reactor standpipe can be calculated. From the calculated pressures at the bottom of the standpipes, the heights of the upper and lower standpipes can be calculated as follows:

$$H_{SP1} = \frac{1}{\rho_B g}(P_2 - P_{SP,out}) \quad (9)$$

$$H_{SP2} = \frac{1}{\rho_B g}\left(P_{SP,out} - P_{AR,out}\right) + (H_2 - H_1) \quad (10)$$

The location of standpipe heights H_{SP1} and H_{SP2} are shown in Figure 2. If the resulting calculation shows that either H_{SP1} or H_{SP2} are higher than the actual pipe height in the system, the standpipe cannot work. With both the pressures and the heights solved, the pressure-height diagram can be plotted to show the pressure distribution in the system. An example plot is shown in Figure 3.

The analysis also considered the back-pressure control valve that are used to set the static pressures in each reactor. The percent opening of the back-pressure control valves dictates the flow coefficient (C_v) for each valve. Given the mass balances calculated previously, with the outlet flowrate known, the corresponding flow coefficient can be calculated from the following relation, assuming non-choked flow (Swagelock, 2016):

$$q = (6950)C_v p_{in}\left(1 - \frac{2\Delta p}{3p_1}\right)\sqrt{\frac{\Delta p}{p_{in}\rho_g T_{in}}} \quad (11)$$

In this case, p_{in} is the static (absolute) pressure of the corresponding reactor, p_1 is atmospheric pressure (1 bar), and ρ_g is the specific gravity of air or nitrogen at atmospheric pressure and temperature. Due to [eq. 11] temperature limitations of the back-pressure control valves, the temperature of the gas is lower, and in this analysis, the temperature is assumed to be 470 K. From the flow coefficient, the corresponding percentage open for the valve is calculated based on the C_v response curve for the corresponding valve. Each valve follows an "equal percentage" response, and the percentage opening V_i fits the manufacturer data through a power law relation: $V_i = \alpha C_{v,i}^n$ where $C_{v,i}$ is the flow coefficient for valve i, α is a constant, and n is an exponent that is between zero and one for the equal-percentage type valve. The effect of the valve percentage opening on the system can be determined through iterative procedure. If the valve percentage open is known, the calculation procedure consists of changing the back pressure until the resulting valve percentage is at the desired value.

Table 2. Parameters proposed to identify similarity in the Seal Pot and associated stand-legs.

Operating property	**Proto-type**	**VL model**	**cold CPO**
T, °C	850	20	20
P, kPa	160	125	110
$\dot{m}_s$, kg/s	0.5	0.7	0.37
m_s, kg	50	150	50
Dimensionless parameters*:			
d_p/D_c +	1.69E-04	0.59	1
ρ_s/ρ_g +	6160	0.53	0.36
Fr +	0.016	0.93	15.1
u_g/u_{mf} +	10.6	1.13	9.02
$G_s/(\rho_s u_g)$ +	0.03	1	2.84
$G_s/(\rho_g u_g)$	182	0.53	1
u_g/u_{tr}	0.059	2.14	1.81
Re	0.633	4.06	1.82
Ar	258	4.59	17.4

**Values of the prototype's dimensionless parameters are for SP bed, while values for the models are model/prototype ratios averaged over all seven streams in Table 3.*
+Parameters used in viscous limit case.

RESULTS AND DISCUSSION

Typical operations are described by Weber et al. (2014) and Bayham et al. (2016) including system startup, the reactor controls used, and objectives for operability. Shadle et al. (2017) describe how significant challenges are associated with solids handling and upsets from losing carrier inventory. Scaling parameters are summarized in Tables 2, 3, and 4. In the Viscous Limit (VL) scaling case the dimensionless numbers for the flows and particles were determined by minimizing the sum of squared differences between those for the prototype hot unit. The RMSE was 0.295, but 95% of the deviation from scaling agreement was in the ratios for d_p/D_c and ρ_s/ρ_g. This case requires obtaining sufficient quantities of a lead oxide powder having the same particle size distribution as the oxygen carrier used in the hot prototype. The other scaling case evaluated was chosen to maintain the same granular material as the unit as well as the load ratio ($G_s/(\rho_g u_g)$, Re, and u_g/u_{tr}. This scaled case is called the cold CPO model, and has an RMSE of 0.598, 80% of which was from the inability to match the latter two dimensionless terms in nearly equivalent proportions. The particle properties for each of these cases and the estimated fluidization velocities are presented in Table 3. The differences in the particle density result in the differences in inventory required for the VL case.

Table 3. Physical and fluidization properties of manufactured oxygen carrier and proposed scaled particle.

Property	units	Hot Prototype	VL Model	cold CPO
d_p,	µm	343	120	343
ρ_{bulk}	kg/m^3	1430	3800	1430
$\rho_{particle}$	kg/m^3	2900	9400	2900
ϕ		0.91	0.91	0.91
u_{mf}	cm/s	1.7	2	4.18
u_t^*	m/s	2.4	2	2.75
u_{tr}^*	m/s	6.6	3.3	3.3

*Calculated using eq. for $u_{tr}^{[i]}$ and $u_t^{[ii]}$

A list of process variables and their nominal conditions at baseline conditions are reported by Shadle et al. (2017). Based upon those and the scaling numbers the flows are presented in Table 4 for each of the gas streams in the hot CLR (prototype) and the cold flow unit (VL and cold CPO). This material was tested in the thermal analysis laboratory and is proposed to be used in the CLR. However, the dimensional analysis using the viscous limit set could be matched quite effectively with the parameters identified in *Table* . The prototype material and the scaled parameter and their estimated fluidization behavior are characterized by differences of about a factor of 3 in diameter, density, and u_{mf} and u_{tr}.

An analysis of the hydrodynamics and estimated bed heights in the prototype indicated that the outlet pressures identified in the base conditions would not sustain a bed level in the cyclone dipleg. This was readily resolved by altering the outlet pressures. A new base case was calculated that produced a minimum bed height of 0.2 m in that dipleg. The same result and adjustments were made in the VL and cold CPO cases. The complete pressure profiles for this is shown in Figure 3 along with the comparable profiles for the cold VL, and CPO model cases.

Table 4. Primary operating conditions for the nominal operating conditions of NETL's CLR.

Vessel	Stream	Proto-type	VL model	cold CPO
Air Reactor	Primary	236	617	169
	Secondary	496	1314	356
Seal Pot	Fluidization	142	364	99
Fuel reactor	Fluidization	236	568	165
	Fuel	28	68	13
L-valve	Aeration	12	28	8
	Sparger	57	135	40

There are notable similarities between the prototype and the scaled cases, but there are also distinct differences. Equal heights were established in the SP, overflow standleg, and the FR. The range of pressures in the prototype were intermediate between the narrow cold CPO and the VL model cases. At the lower pressures the CPO model could not achieve as high a pressure differential between the SP and AR outlets to build a fluid bed in the cyclone dipleg. The constraint in these calculations was the back pressure control valve on the AR cyclone outlet. This valve was fully opened before it was able to release enough flow or pressure necessary to build as high a bed in the dipleg feeding the SP. In the VL model the higher particle density generated much greater pressure even though the bed height was only 1/3 that in the prototype because of the higher flows defined in this scaling approach. The VL scaling option produces much higher *Re* than the prototype. This was still within the viscous regime, i.e. *Re*<4 for the moving and bubbling fluidized bed portions of the CLR loop; however, the Re exceeded this in several vessels of the VL case – and in all cases for the AR riser and crossover. The riser and crossover were necessarily operated in the transport regimes. In the protoype and CPO model conditions the *Re* values in the riser and crossover were on the order of 30 and 60, respectively; *Re* values were quadruple these for the VL model conditions. For the AR the *Re* exceeded 4 for only the VL flow conditions, being 7 and 16 respectively; however; in the SP, FR, and standlegs, which are considered the source of the process instabilities, the *Re* were all well within this viscous regime.

Figure 3. Pressure profile for Hot CLR and scaled models for CPO.

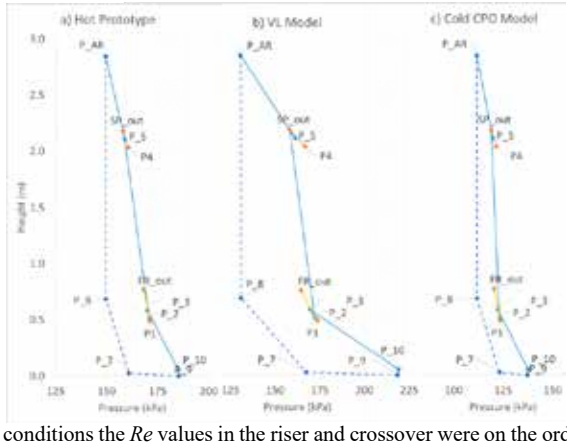

The impact of back-pressure control valves on these bed levels and gas flows was studied for the prototype conditions. The AR back pressure valve, V_3, has little impact on the overflow standleg, H_{SP1}, but opening it from 72 to 76% was sufficient to increase the dipleg height (H_{SP2}) over the full operating range, 0 to 1 m.

Likewise, back pressure valve on the outlet of the FR, V_1, had little impact on the dipleg height, H_{SP1}, but the closing it from 36 to 32% was enough to increase the standleg below the SP over its full operating range. The SP back pressure control valve, V_2, affected these two standleg heights in opposite direction. Opening V_2 from 79 to 83.5% increased H_{SP1} and decreased H_{SP2}. H_{SP1} increased only to half of the available height while H_{SP2} bed level dropped until it was completely lost. Different flows and valve settings would likely alter these respective effects.

Understanding the process changes that affect the gas velocities in the standlegs was considered critical to controlling the process and avoiding unexpected process upsets. In addition to effecting standpipe bed levels, changes in the SP back pressure control valve, V_2, influenced the gas flow in both the cyclone dipleg (u_{g2}) and overflow standleg (u_{g1}) (Figure 4). The gas flow was co-current with solids flows in both standlegs in downward directions. Due to the flow convention used in developing the force balance expressions in which positive direction is defined by the arrow direction. The downward flows likely would produce sufficient force to overcome the particle-wall frictional forces maintaining the bed levels. Additional analysis is required to quantify the stability of these conditions.

Figure 4. Sensitivity of gas velocities in standlegs around the SP to changes in the SP outlet valve. V2.

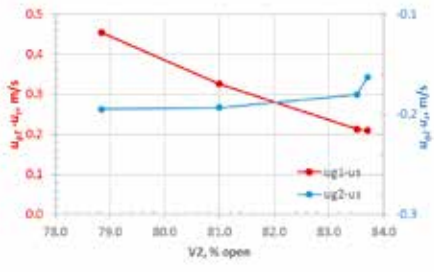

CONCLUSION

Analysis of the FB-CLR system was used to identify he operating range of the hot prototype and scaled models of it. The scaling parameters were critically evaluated identifying strengths and weaknesses in the analysis. Expressions were developed from conservation of mass and forces were used to estimate the flows and bed heights resulting from operating the control valves at the outlet of the process. This analysis was extended to identify the operating range based on bed levels. Further analysis of these effects and experimental validation is required to demonstrate the potential improvements that can be made to the process. Changes in the SP back pressure control valve exhibited influence over both the cyclone dipleg and overflow. Future work is planned to identify the best estimation approach to tackle such a control problem between the hot and the cold unit. During future test operations the data from the shifting solids inventory in the cyber-physical unit will be used to control some of the fluidizing and solids motive gas flows, as well as, the back pressure control valves within the hot pilot plant facility to increase the operating range of the test facility and minimize the risk of process upsets due to flow reversal.

With this additional information on operating states and constraints the protoype system (FB-CLR) can be more completely identified and controls can be developed to maintain process stability or make smooth transitions between operating conditions. A network architecture was identified to share and integrate this information between to the two systems, based upon experiences in operating a cyber-physical fuel cell – turbine hybrid (Tucker et al, 2014; Shelton et al., 2005). Fail-safe controls transitions can then be automated making more efficient, though inherently less robust components practicable.

NOTATION

A-C	Matrix coefficients
A	area [m^2]
AR	Air Reactor
C	Coefficient for flow [Eq. 11]
CPO	Cyber physical Observer
FB	Fluidized Bed
CLR	Chemical Looping Reactor
NETL	National Energy Technology Laboratory
m	mass inventory
d	stochiometric factor for fuel combustion reaction
d_p	diameter of particle [microns]
F	Flow [lpm]
FB	Fluidized Bed
FR	Fuel Reactor
H	Height
k	gain factor
L	Length, characteristic
$\dot{m}$	mass flow rate [kg/s]
$\dot{m}_{oc}$	characteristic circulation rate for an oxygen carrier
M	Metal in oxygen carrier [eq. Ca, Fe, Cu, Ni]
MW	Molecular Weight
na	Not available
p_1	pressure [bar]
P	Pressure [kPa]
q	volumetric flow through a valve [M^3/s, Eq. 11]
R	Resistance [Eq. 6, 7] or Oxygen transport capacity[]
Re	Reynold's No. , $\frac{\rho_g u_g d_p}{\mu}$
r	internal rate
SP	Seal-Pot
t	time
T	temperature [K] or [°C]

u	inputs vector
u	velocity, cm/s
V	*V*alve position
x	states vector
X	Conversion
y	outputs vector

Greek symbols

α	valve flow constant
β	gas solid drag coefficient
Δ	Heat
ΔH_c^o	Heat of the gas fuel combustion (kJ/mol)
Δp	pressure differential [kPa]
μ	viscosity [kg/m-s]
ρ	density [kg/m3]
Φ	Reactivity, characteristic
ϕ	sphericity
τ	time for complete conversion

Subscripts and superscripts

1-20, i	stream numbers [Fig 1 and 2]
o	Reference locations [Eq. 3]
AR	Air Reactor
bulk	bulk as in average properties of a bed of particles
FR	Fuel Reactor
g	gas phase
in, out	inward or outward flow direction
LV	Non mechanical L-valve
mf	at minimum fluidization conditions
n	valve flow exponent [between 0 and 1 for equal percentage valve type]
p	particle
plenum	space below fluid bed distributor
standpipe	column of solids moving by gravity
s	solid phase
sec	secondary air
SP	Seal-Pot
SPG	Sparger aeration in L-valve
t	terminal as in after accelerating
tr	transition or transport velocity
v	valve
x, y	stoichiometric coefficient

REFERENCES

Abad, A., Adánez, J., García-Labiano, F., de Diego, L.F., Gayán, P., Celaya, J. 2007, Mapping of the range of operational conditions for Cu-, Fe-, and Ni-based oxygen carriers in chemical-looping combustion, Chem. Eng. Sci. 62, 533–549.

Bayham, S. et al. 2016,

Cabello, A., Abad, A., García-Labiano, F., Gayán, P., de Diego, L.F., Adánez, J. 2014, Kinetic determination of a highly reactive impregnated Fe2O3/Al2O3 oxygen carrier for use in gas-fueled Chemical Looping Combustion, Chemical Engineering Journal, 258, 265–280.

Glicksman, L. R., 1984, Scaling relationships for fluidised beds, Chemical Engineering Science, 39, 1373-1379

Glicksman, L. R., 1988, Scaling relationships for fluidised beds, Chemical Engineering Science, 43, 1419-1421

Lee, E. A. and S. A. Seshia, 2011, Introduction to Embedded Systems, A Cyber-Physical Systems Approach, http://LeeSeshia.org, ISBN 978-0-557-70857-4. http://cyberphysicalsystems.org/

Ommen, J.R.van, S.Sijbesma, J.Nijenhuis, B.G.M. van Wachem, 2005, "Computational Validation of the Scaling Rules for Fluidized Bed", Journal???

Richards, G; Straub, D; Weber, J; Breault, R; Chorpening, B; Siriwardane, R., 2014, "Chemical Looping Combustion – research for power and process heat applications" American Flame Research Committee 2014 Industrial Combustion Symposium, Houston, Texas, USA, Sept. 7-10.

Richards, G. A., D. Straub, J. Weber, R. Breault, B. Chor-pening, R.Siriwardane, 2014, "Chemical Looping Combustion – Research for Power and Process Heat Applications", American Flame Research Committee, Industrial Combustion Symposium, September 7 , Houston, Texas

Ruzicka, M.C., 2008, "On dimensionless numbers", *Chemical Engineering Research and Design*, *86*, 835-868

Shadle, LJ., P. Pezzini, E.R. Monazam, J. Weber, S. Bayham, D. Tucker, R. Breault, R.Panday, K.M. Bryden, "Cyber-Physical Observer For Fluid Bed-Chemical Looping Control Applications", 2017 ASME Turbo Expo, 6-9 June 2005, Charleston, SC, USA, GT2017-64881.

Shelton, M. S.; Liese, E.; Tucker, D.; Celik, I. "A Study in the Process Modeling of the Startup of Fuel Cell/Gas Turbine Hybrid Systems," 2005 ASME Turbo Expo, 6-9 June 2005, Reno, NV, USA, GT2005-68466.

Swagelok, 2016, "Valve Sizing Technical Bulletin", found at https://www.swagelok.com/downloads/webcatalogs/EN/MS-06-84.pdf

Tucker, D.; Abreu-Sepulveda, M. A.; Harun, N. F. "SOFC Lifetime Assessment in Gas Turbine Hybrid Power Systems," Journal of Fuel Cell Science and Technology, 11 (5): 051008 (October 2014); doi: 10.1115/1.4028953

Weber, J; Straub, D; Bayham, S; and Breault, R., 2016 "Operating experience of a 50 kWth methane chemical looping reactor" Proceedings of the XV International Fluidization Conference, Montreal, Canada, May 25. ECI Publishing, pp. 16.